Supporting Information for

# Multi-Responsive Spin-Crossover Driven by Rotation of Tetraphenylborate Anion in an Iron(III) Complex

Si-Guo Wu,[†1] Md. Najbul Hoque,[†1] Jie-Yu Zheng,[1] Guo-Zhang Huang,[1] Nguyen Vu Ha Anh,[2] Liviu Ungur,[2] Wei-Xiong Zhang,[1] Zhao-Ping Ni*[1] & Ming-Liang Tong*[1]

[1] Province Key Laboratory of Bioinorganic and Synthetic Chemistry of Ministry of Education, School of Chemistry, Sun Yat-Sen University, Guangzhou 510275, P. R. China.

[2] Department of Chemistry, National University of Singapore, Block S8 Level 3, 3 Science Drive 3, Singapore 117543.

*Corresponding Author(s): nizhp@mail.sysu.edu.cn; tongml@mail.sysu.edu.cn.

**DOI: 10.1002/anie.2016XXXXX**

# Content

## Experimental Procedures

**Materials and General Methods.** The precursor $Fe^{III}$(salten)Cl ($H_2$salten = 4-azahetane-1,7-bis(salicylideneiminate)) and the ligand TPB·2$H_2O$ (TPB = 1,2,4,5-tetra(4-pyrideyl) benzene) were synthesized as literature described.[1,2] All the reagents and solvents were commercially available and used without further purification.

**Elemental analyses** on C, H, N were carried out with an Elementar Vario-EL CHNS elemental analyzer.

**Powder X-ray diffraction (PXRD)** patterns were performed on Bruker D8 Advance Diffratometer (Cu-$K_\alpha$, $\lambda$ = 1.54056 Å).

**The FT-IR spectra** were recorded on Thermo Scientific Nicolet 6700-Contiuμm instrument in KBr tablets in the range of 4000~400 $cm^{-1}$.

**Thermogravimetric analyses (TG)** were carried out on a TA Instrument NETZSCH TG 209 F3 under flowing nitrogen at a heating rate of 10 °C/min.

**Differential Scanning Calorimetry (DSC)** was performed on the samples within an aluminium crucible using a NETZSCH5 with a sweeping rate of 10 K $min^{-1}$ under $N_2$ atmosphere.

**Magnetic susceptibility measurements** were performed with a Quantum Design MPMS XL-7 SQUID magnetometer working under an applied field of 2000 Oe. Polycrystalline samples were embedded in vaseline to prevent torqueing. Data were corrected for the diamagnetic contribution calculated from Pascal's constants.

**Crystallography.** Single Crystal X-ray measurements were performed with Bruker D8 QUEST diffractometer equipped with APEXIII CCDII (Mo-$K_\alpha$ radiation, $\lambda$ = 0.71073 Å). The data indexing and integration were carried out with Bruker Smart program. The structures were solved by direct methods using SHELXTL[3] and all non-hydrogen atoms were refined with anisotropic displacement parameters by least-squares on weighted $F^2$ values. The hydrogen atoms were constrained to idealised geometries using a riding model. CCDC contain the supplementary crystallographic data for this paper. These data can be obtained free from The Cambridge Crystallographic Data Centre via https://www.ccdc.cam.ac.uk/structures/.

**Dielectric spectroscopy.** The dielectric measurements were carried on microcrystal samples by a TH2828A impedance analyzer with a sweep rate of 2 K $min^{-1}$ in a Mercury iTC cryogenic environment controller of Oxford Instrument.

## Synthesis

**[{$Fe^{III}$(salten)}$_2$(TPB)](BPh$_4$)$_2$** (**I**): $Fe^{III}$(salten)Cl (0.5 mmol, 213.5 mg) and TPB·2$H_2O$ (0.25 mmol, 106 mg) were dissolved in 30 ml EtOH at 70 °C for 1 hour. After cooling down to room temperature, 10 ml EtOH solution of $NaBPh_4$ (0.5 mmol, 171 mg) was added to the mixture which resulted in large amount of black precipitate immediately. The mixture was filtered to remove the precipitate and the filtrate was transferred into a 40 ml vial with sealing. The black block crystals were collected after one day. Yield: 80 mg, 17.7%. Anal. Calcd for $C_{114}H_{104}B_2Fe_2N_{10}O_4$ (**I**): C, 75.59; H, 5.79; N, 7.73. Found: C, 75.13; H, 5.82; N, 7.76. IR spectra (KBr, $cm^{-1}$): 3216 (m), 3061 (m), 1936 (w), 1615 (s), 1543 (s), 1469 (m), 1444 (s), 1389 (m), 1331 (m), 1299 (s), 1210 (m), 1152 (m), 1126 (m), 1064 (m), 1032 (m), 888 (m), 844(m), 820 (m), 788 (m), 766 (s), 732 (s), 707 (s), 604 (s), 568 (m), 544 (m), 445 (m).

**II phase**: Complex **I** was kept in an oven at 380 K for 2 hours. Anal. Calcd for $C_{114}H_{104}B_2Fe_2N_{10}O_4$ (**II**): C, 75.59; H, 5.79; N, 7.73. Found: C, 75.40; H, 5.66; N, 7.68. IR spectra (KBr, $cm^{-1}$): 3245 (m), 3056 (m), 1936 (w), 1612 (s), 1547 (s), 1469 (m), 1420 (s), 1390 (m), 1294 (s), 1206 (m), 1152 (m), 1122 (m), 1064 (m), 1032 (m), 911 (m), 837(m), 820 (m), 788 (m), 766 (s), 728 (s), 707 (s), 609 (s), 563 (m), 544 (m) and 445 (m).

**III phase**: The heating phase **II** was exposed to water vapor for two days to obtain the water induced phase **III**. Anal. Calcd for $C_{114}H_{104}B_2Fe_2N_{10}O_4$ (**III**): C, 75.59; H, 5.79; N, 7.73. Found: C, 75.90; H, 5.71; N, 7.62. IR spectra (KBr, $cm^{-1}$): 3250 (m), 3051 (m), 1941 (w), 1616 (s), 1541 (s), 1468 (m), 1442(s), 1420 (s), 1394 (m), 1298 (s), 1202 (m), 1152 (m), 1125 (m), 1065 (m), 1028 (m), 908 (m), 836(m), 820 (m), 792 (m), 766 (s), 731 (s), 707 (s), 610 (s), 562 (m), 544 (m) and 445 (m).

**IV phase**: The heating phase complex (**II**) was exposed to EtOH vapor for two days to obtain the ethanol induced phase **IV**. Anal. Calcd for $C_{114}H_{104}B_2Fe_2N_{10}O_4$ (**IV**): C, 75.59; H, 5.79; N, 7.73. Found: C, 75.31; H, 5.69; N, 7.58. IR spectra (KBr, $cm^{-1}$): 3249 (m), 3051 (m), 1932 (w), 1616 (s), 1546 (s), 1469 (m), 1446(s), 1418 (s), 1390 (m), 1293 (s), 1204 (m), 1152 (m), 1123 (m), 1066 (m), 1036 (m), 906 (m), 839(m), 819 (m), 790 (m), 765 (s), 728 (s), 703 (s), 608 (s), 563 (m), 540 (m) and 448 (m).

## Results and Discussion

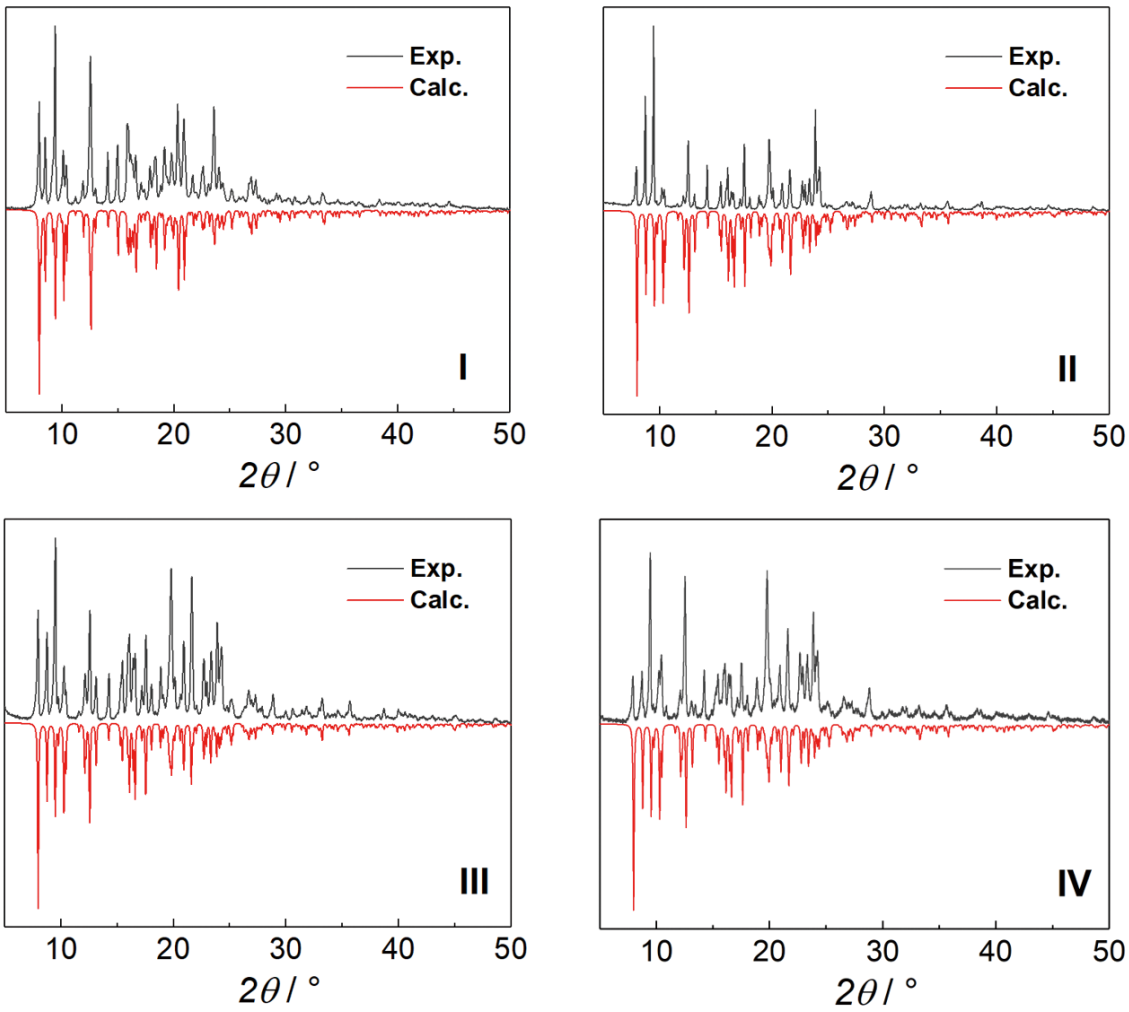


**Figure S1.** Experimental and simulated powder X-ray diffraction (PXRD) patterns for **I**–**IV**.

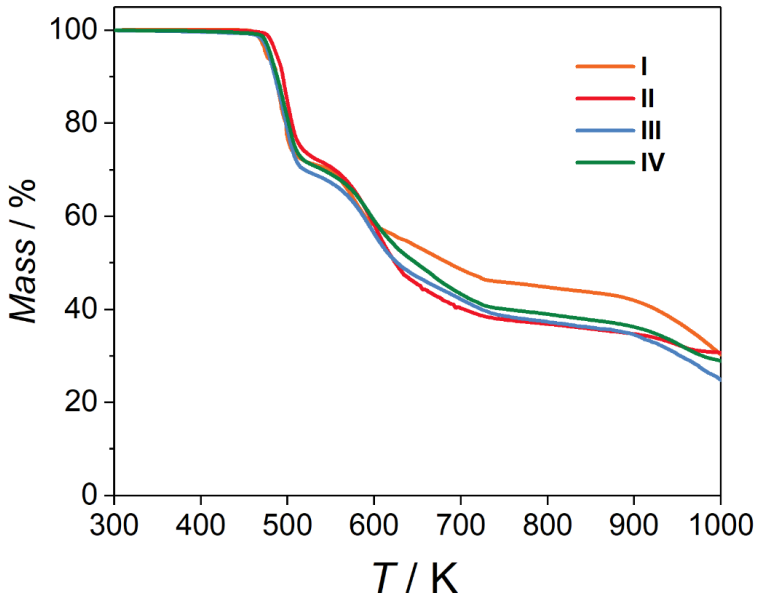


**Figure S2.** Thermogravimetric analysis (TGA) curve of **I**–**IV** at a heating rate of 10 K $min^{-1}$.

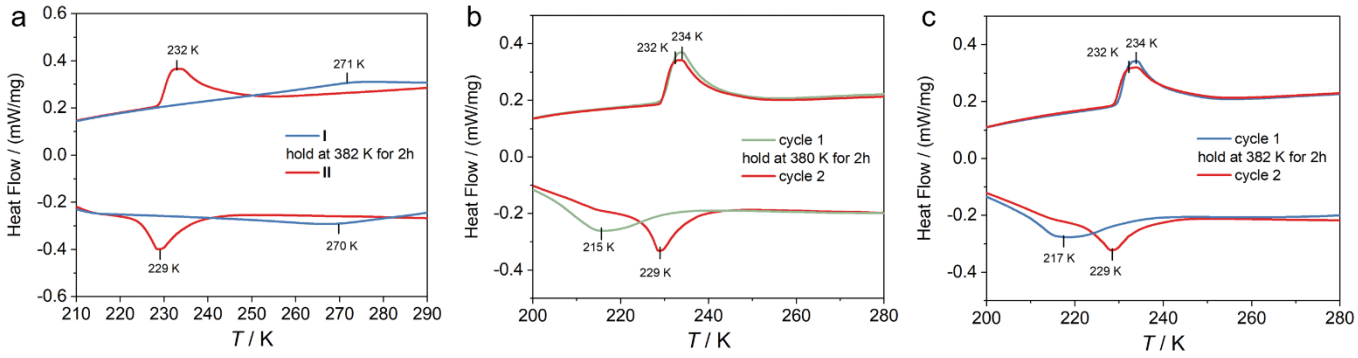


**Figure S3.** Differential Scanning Calorimetry (DSC) measurements of a) **I** → **II**, b) **III** → **II** and c) **IV** → **II**.

**Table S1.** Crystallographic data and structural refinements for **I** at different temperatures.

| Compound | 120 K | 298 K |
|---|---|---|
| Formula | $C_{114}H_{104}B_2Fe_2N_{10}O_4$ | |
| Formula weight | 1811.39 | |
| Crystal system | Triclinic | |
| Space group | *P*-1 | |
| *a* / Å | 11.6183(7) | 11.5542(11) |
| *b* / Å | 11.2084(6) | 11.1678(10) |
| *c* / Å | 18.5870(10) | 19.1907(17) |
| *α* / ° | 84.4585(16) | 85.071(2) |
| *β* / ° | 79.3393(16) | 79.098(2) |
| *γ* / ° | 74.6007(16) | 77.632(2) |
| *V* / Å$^3$ | 2323.7(2) | 2372.5(4) |
| *Z* | 1 | |
| $\rho_{calcd.}$ (g/cm$^3$) | 1.294 | 1.266 |
| *μ* (mm$^{-1}$) | 0.374 | 0.366 |
| *F* (000) | 952.0 | 952.0 |
| Reflections collected | 53677 | 54459 |
| Independent reflections | 10660 | 10829 |
| GOF on $F^2$ | 1.029 | 1.010 |
| $R_1$, $wR_2$ [$I \geq 2\sigma(I)$][a] | 0.0480, 0.0948 | 0.0702, 0.1522 |
| $R_1$, $wR_2$ (all data) | 0.0900, 0.1076 | 0.1772, 0.1914 |
| Largest diff. peak/hole / e Å$^{-3}$ | 0.51 /-0.50 | 0.52 /-0.37 |
| CCDC No. | 1980012 | 1980015 |

[a] $R_1 = \sum||F_o| - |F_c||/\sum|F_o|$. $wR_2 = [\sum w(F_o^2 - F_c^2)^2/\sum w(F_o^2)^2]^{1/2}$.

**Table S2.** Crystallographic data and structural refinements for **II** at different temperatures.

| Compound | 120 K | 298 K |
|---|---|---|
| Formula | $C_{114}H_{104}B_2Fe_2N_{10}O_4$ | |
| Formula weight | 1811.39 | |
| Crystal system | Triclinic | |
| Space group | *P*-1 | |
| *a* / Å | 11.2731(5) | 11.3792(5) |
| *b* / Å | 11.3227(6) | 11.3615(5) |
| *c* / Å | 18.5890(9) | 18.9580(8) |
| *α* / ° | 81.403(2) | 81.2766(13) |
| *β* / ° | 85.927(2) | 81.5483(13) |
| *γ* / ° | 75.837(2) | 79.2079(14) |
| *V* / Å$^3$ | 2273.30(19) | 2361.97 (18) |
| *Z* | 1 | |
| $\rho_{calcd.}$ (g/cm$^3$) | 1.323 | 1.273 |
| *μ* (mm$^{-1}$) | 0.382 | 0.368 |
| *F* (000) | 952.0 | 952.0 |
| Reflections collected | 43291 | 44062 |
| Independent reflections | 10395 | 8661 |
| GOF on $F^2$ | 1.032 | 1.013 |
| $R_1$, $wR_2$ [$I \geq 2\sigma(I)$][a] | 0.0388, 0.0839 | 0.0421, 0.0920 |
| $R_1$, $wR_2$ (all data) | 0.0603, 0.0912 | 0.0702, 0.1031 |
| Largest diff. peak/hole / e Å$^{-3}$ | 0.27 /-0.44 | 0.22 /-0.27 |
| CCDC No. | 1980009 | 1980011 |

[a] $R_1 = \sum||F_o| - |F_c||/\sum|F_o|$. $wR_2 = [\sum w(F_o^2 - F_c^2)^2/\sum w(F_o^2)^2]^{1/2}$.

**Table S3.** Crystallographic data and structural refinements for **III** at different temperatures.

| Compound | 120 K | 298 K |
|---|---|---|
| Formula | $C_{114}H_{104}B_2Fe_2N_{10}O_4$ | |
| Formula weight | 1811.39 | |
| Crystal system | Triclinic | |
| Space group | *P*-1 | |
| *a* / Å | 11.2740(10) | 11.398(3) |
| *b* / Å | 11.3038(10) | 11.389(3) |
| *c* / Å | 18.6481(17) | 19.008(5) |
| *α* / ° | 81.113(3) | 81.260(7) |
| *β* / ° | 85.841(3) | 81.569(7) |
| *γ* / ° | 75.891(2) | 78.987(7) |
| *V* / Å$^3$ | 2275.6(4) | 2376.2(11) |
| *Z* | 1 | |
| $\rho_{calcd.}$ (g/cm$^3$) | 1.322 | 1.266 |
| *μ* (mm$^{-1}$) | 0.382 | 0.366 |
| *F* (000) | 952.0 | 952.0 |
| Reflections collected | 45029 | 47674 |
| Independent reflections | 9366 | 10088 |
| GOF on $F^2$ | 1.023 | 1.011 |
| $R_1$, $wR_2$ [$I \geq 2\sigma(I)$][a] | 0.0504, 0.0947 | 0.0584, 0.1106 |
| $R_1$, $wR_2$ (all data) | 0.0981, 0.1093 | 0.1489, 0.1377 |
| Largest diff. peak/hole / e Å$^{-3}$ | 0.32 /-0.45 | 0.23 /-0.51 |
| CCDC No. | 1980014 | 1980013 |

[a] $R_1 = \sum||F_o| - |F_c||/\sum|F_o|$. $wR_2 = [\sum w(F_o^2 - F_c^2)^2/\sum w(F_o^2)^2]^{1/2}$.

**Table S4.** Crystallographic data and structural refinements for **IV** at different temperatures.

| Compound | 120 K | 298 K |
|---|---|---|
| Formula | $C_{114}H_{104}B_2Fe_2N_{10}O_4$ | |
| Formula weight | 1811.39 | |
| Crystal system | Triclinic | |
| Space group | *P*-1 | |
| *a* / Å | 11.2656(11) | 11.374(2) |
| *b* / Å | 11.2898(10) | 11.321(2) |
| *c* / Å | 18.6004(17) | 18.954(3) |
| *α* / ° | 81.173(3) | 81.371(5) |
| *β* / ° | 85.993(3) | 81.581(5) |
| *γ* / ° | 75.857(3) | 78.987(5) |
| *V* / Å$^3$ | 2265.5(4) | 2350.9(7) |
| *Z* | 1 | |
| $\rho_{calcd.}$ (g/cm$^3$) | 1.328 | 1.279 |
| *μ* (mm$^{-1}$) | 0.384 | 0.370 |
| *F* (000) | 952.0 | 952.0 |
| Reflections collected | 42057 | 41789 |
| Independent reflections | 9290 | 9530 |
| GOF on $F^2$ | 1.069 | 1.052 |
| $R_1$, $wR_2$ [$I \geq 2\sigma(I)$][a] | 0.0562, 0.1004 | 0.0655, 0.1164 |
| $R_1$, $wR_2$ (all data) | 0.1089, 0.1158 | 0.1405, 0.1437 |
| Largest diff. peak/hole / e Å$^{-3}$ | 0.30 /-0.49 | 0.26 /-0.40 |
| CCDC No. | 1980008 | 1980010 |

[a] $R_1 = \sum||F_o| - |F_c||/\sum|F_o|$. $wR_2 = [\sum w(F_o^2 - F_c^2)^2/\sum w(F_o^2)^2]^{1/2}$.

**Table S5.** Selected structural parameters for **I**−**IV** at different states.

| Parameter | **I** (120 K) | **I** (298 K) | **II** (120 K) | **II** (298 K) | **III** (120 K) | **III** (298 K) | **IV** (120 K) | **IV** (298 K) |
|---|---|---|---|---|---|---|---|---|
| Fe1−N1 | 2.0047(19) | 2.143(3) | 2.0285(14) | 2.1987(19) | 2.027(2) | 2.196(3) | 2.021(2) | 2.193(3) |
| Fe1−N2 | 1.9679(18) | 2.066(4) | 1.9546(14) | 2.0910(19) | 1.953(2) | 2.091(3) | 1.954(2) | 2.090(3) |
| Fe1−N3 | 1.9605(18) | 2.059(4) | 1.9533(14) | 2.0780(19) | 1.950(2) | 2.075(3) | 1.947(2) | 2.074(3) |
| Fe1−N4 | 2.0020(16) | 2.151(3) | 2.0071(14) | 2.1986(16) | 2.003(2) | 2.202(2) | 2.003(2) | 2.199(3) |
| <Fe−N>[a] | 1.9838(18) | 2.105(4) | 1.9859(14) | 2.1416(18) | 1.983(2) | 2.141(3) | 1.981(2) | 2.139(3) |
| Fe1−O1 | 1.8793(15) | 1.904(3) | 1.8854(12) | 1.9213(16) | 1.8800(18) | 1.924(2) | 1.881(2) | 1.919(3) |
| Fe1−O2 | 1.8766(16) | 1.915(3) | 1.8789(11) | 1.9188(15) | 1.8773(17) | 1.925(2) | 1.8763(19) | 1.919(2) |
| <Fe−O>[b] | 1.8780(16) | 1.909(3) | 1.8822(12) | 1.9201(16) | 1.88787(18) | 1.925(2) | 1.8777(20) | 1.919(3) |
| <O1−Fe1−O2>[c] | 176.94(7) | 173.41(11) | 177.68(5) | 169.47(7) | 177.68(8) | 169.53(9) | 177.74(9) | 169.59(11) |
| ∑Fe[d] | 17.01 | 38.43 | 15.48 | 54.26 | 15.40 | 54.33 | 15.56 | 53.48 |
| Fe···Fe[e] | 15.3664(8) | 15.6328(10) | 15.4051(8) | 15.7639(7) | 15.4023(12) | 15.7966(32) | 15.3837(12) | 15.7557(22) |
| anion(B)…Fe[f] | 7.4664(26) | 7.1988(5) | 7.4308(24) | 7.1038(32) | 7.4282(38) | 7.139(4) | 7.4191(38) | 7.0998(51) |

[a]The average Fe−N bond lengths (Å); [b]The average Fe-O bond lengths (Å); [c]The angle of O1−Fe1−O2 (°); [d]Octahedral distortion parameters (°); [e]The intramolecular Fe···Fe distance; [f]The distance of B1···Fe1.

**Table S6.** The comparison of intermolecular interactions among **I**−**IV**.

| Parameter | | **I** (120 K) | **I** (298 K) | **II** (120 K) | **II** (298 K) | **III** (120 K) | **III** (298 K) | **IV** (120 K) | **IV** (298 K) |
|---|---|---|---|---|---|---|---|---|---|
| C24-H24…π (edge-to-face) | $Z^a$ / Å | 4.7085(2) | 4.7654(3) | 4.4795(2) | 4.6134(1) | 4.4800(3) | 4.6315(9) | 4.4678(3) | 4.6019(6) |
| | $r^b$ / Å | 1.686 | 1.834 | 1.781 | 2.000 | 1.778 | 2.021 | 1.792 | 2.038 |
| | $l^c$ / Å | 2.8839(1) | 2.9239(2) | 2.7245(1) | 2.7881(1) | 2.7244(2) | 2.7930(5) | 2.7229(2) | 2.7796(3) |
| | $\theta^d$ / ° | 45.90 | 45.26 | 37.43 | 38.68 | 37.51 | 38.67 | 37.11 | 38.17 |
| C37−H37···π / Å | | 3.4947(1) | 3.4229(2) | 3.6291(1) | 3.5967(1) | 3.6354(2) | 3.6020(7) | 3.6266(3) | 3.5831(4) |
| N1−H1A···π[e] / Å | | 3.3568(1) | 3.4965(2) | – | – | – | – | – | – |
| N1−H1···π[f] / Å | | 3.6439(2)[h] | 3.6490(3)[h] | 2.9235(1) | 2.9518(1) | 2.9233(3) | 2.9698(8) | 2.9086(3) | 2.9508(5) |
| C10−H10···π[e] / Å | | 2.9599(1)[i] | 3.0989(2)[i] | 3.2547(1) | 3.5359(1) | 3.2604(2) | 3.5414(7) | 3.2531(2) | 3.5247(4) |
| C10−H10···π[f] / Å | | 2.7061(1)[j] | 3.2810(2)[j] | 3.3939(1) | 3.7595(1) | 3.4426(3) | 3.7656(8) | 3.4447(3) | 3.7706(5) |
| C3−H3···π / Å | | 3.7130(2) | 3.8646(3) | 3.5567(2) | 4.4869(2) | 3.5669(3) | 4.4945(11) | 3.5504(3) | 4.4932(7) |
| C27−H27···π / Å | | 3.3927(1) | 3.2981(2) | 3.6219(1) | 3.4030(1) | 3.6128(3) | 3.4110(7) | 3.6296(3) | 3.4025(4) |
| C32−H32···N5 / Å | | 2.6096(17) | 3.0768(2) | 2.6070(14) | 3.3752(21) | 2.6126(20) | 3.3736(32) | 2.603(2) | 3.3519(37) |
| C5−H5···N5 / Å | | 2.4325(17) | 2.4316(2) | 2.5271(15) | 2.3974(20) | 2.5333(22) | 2.4088(33) | 2.5297(23) | 2.3936(33) |
| distance of py[g] | | 3.9167(27) | 4.2012(4) | 3.9045(22) | 4.2704(30) | 3.9018(31) | 4.2744(46) | 3.8999(31) | 4.2499(59) |

[a]The distance between the centroids of the corresponding aromatic rings; [b]The offset distance between the centroids of the corresponding aromatic rings; [c]The distance between hydrogen ion and the centroid of aromatic ring; [d]The dihedral angle between two aromatic rings; [e]The aromatic ring C40**−**C45; [f]The aromatic ring C15**−**C20; [g]The distance between the centroids of non-coordinate pyridines of the adjacent TPB ligand; [h]The N1-H1B···π for **I**; [i]The C10B-H10D···π interaction for **I**; [j]The C10A-H10A···π interaction for **I**.

**Table S7.** Potential solvent volume in **I**–**IV** at different states calculated by the Platon program.

| | parameter | **I** | | **II** | | **III** | | **IV** | |
|---|---|---|---|---|---|---|---|---|---|
| | | 120 K | 298 K | 120 K | 298 K | 120 K | 298 K | 120 K | 298 K |
| Platon | voids in unit cell [Å$^3$] | 16.5 | 42.1 | 0 | 46.8 | 0 | 46.9 | 0 | 46.0 |
| | Precentage of voids within the total unit cell volume [%] | 0.7 | 1.8 | 0 | 2.0 | 0 | 2.0 | 0 | 2.0 |

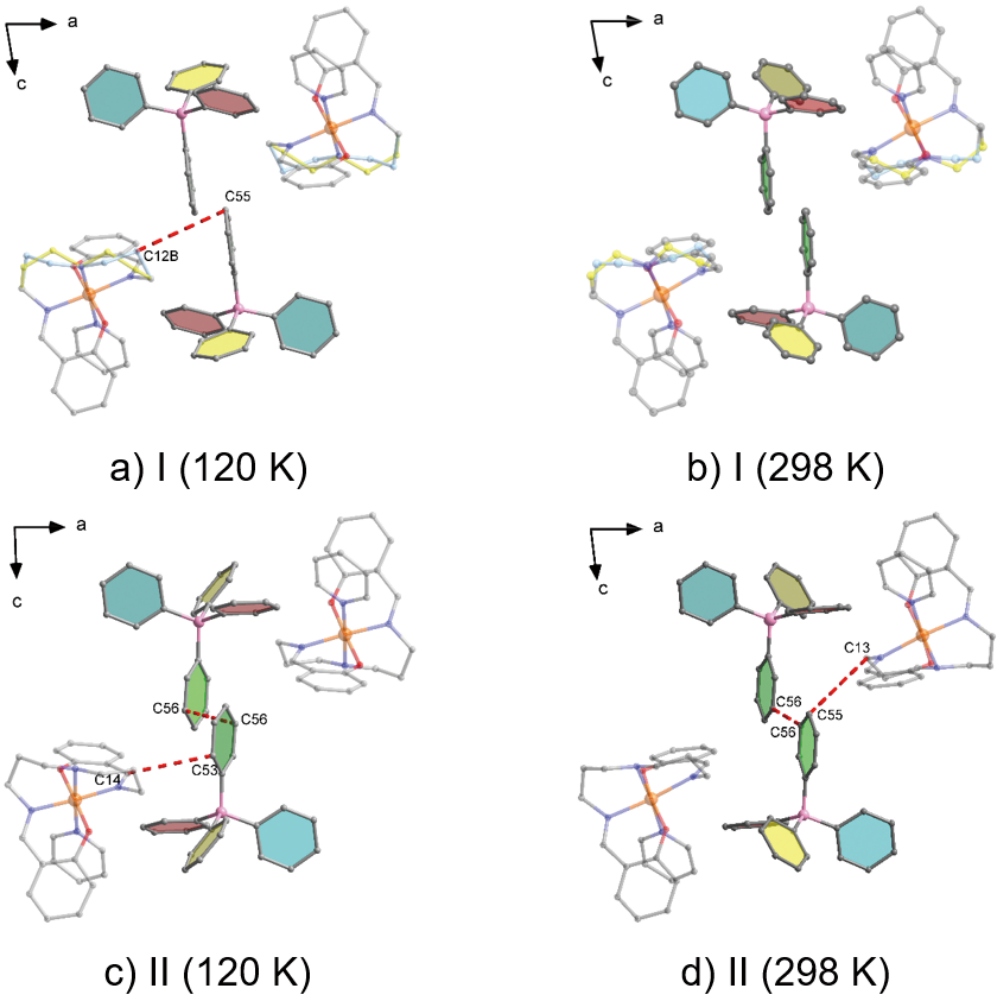


**Figure S4.** The intermolecular interactions between phenyl (C52−C57) of $BPh_4^-$ anion and the adjacent $[\{Fe^{III}(salten)\}_2(TPB)]^{2+}$ for a) **I** at 120 K, b) **I** at 298 K, c) **II** at 120 K and d) **II** at 298 K.

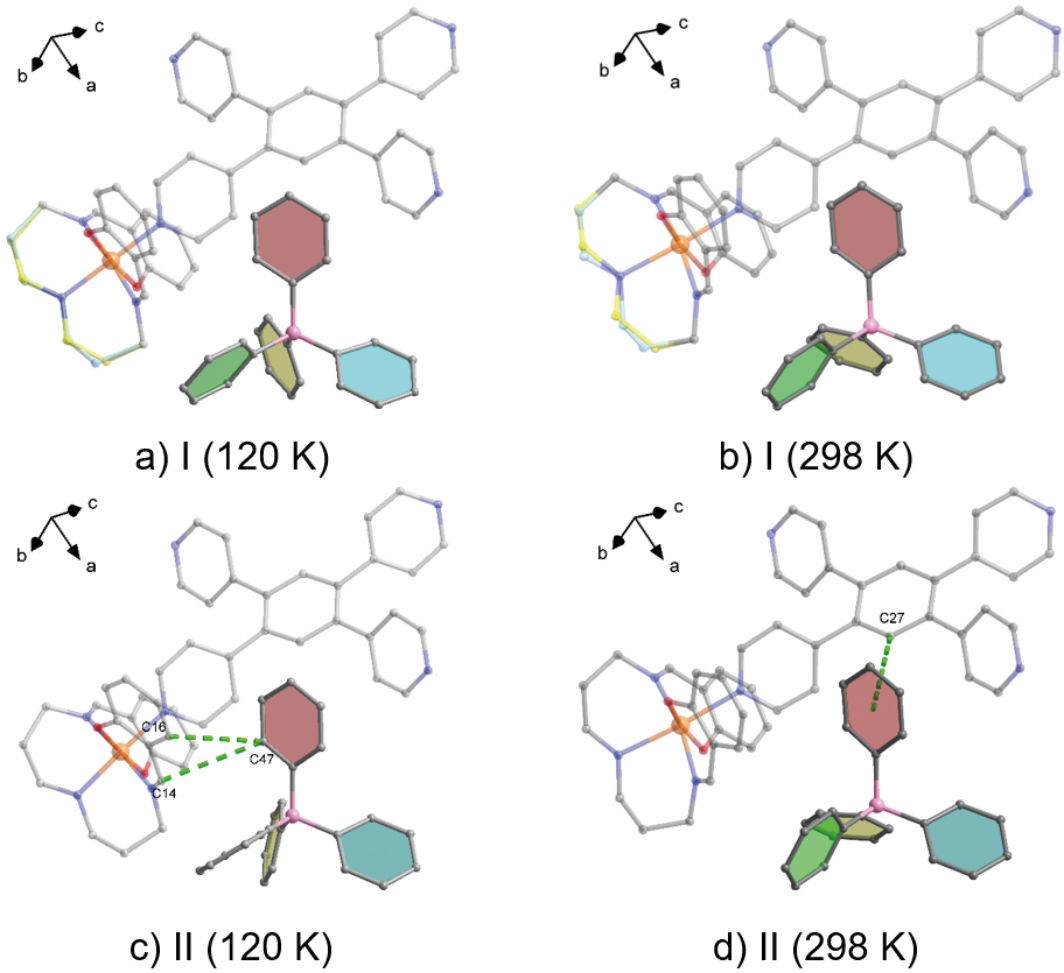


**Figure S5.** The intermolecular interactions between phenyl (C46−C51) of $BPh_4^-$ anion and the adjacent $[\{Fe^{III}(salten)\}_2(TPB)]^{2+}$ for a) **I** at 120 K, b) **I** at 298 K, c) **II** at 120 K and d) **II** at 298 K.

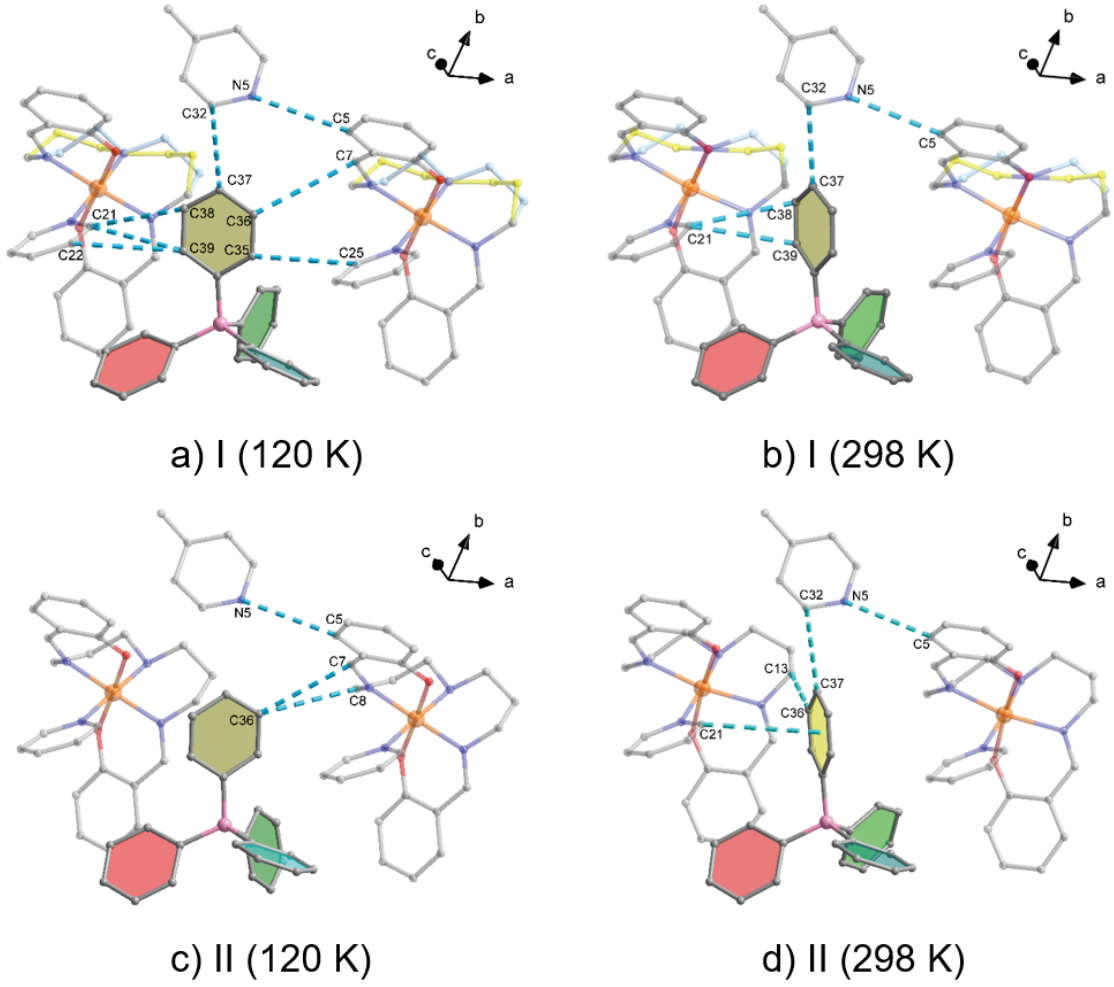


**Figure S6.** The intermolecular interactions between phenyl (C34−C39) of $BPh_4^-$ anion and the adjacent $[\{Fe^{III}(salten)\}_2(TPB)]^{2+}$ for a) **I** at 120 K, b) **I** at 298 K, c) **II** at 120 K and d) **II** at 298 K.

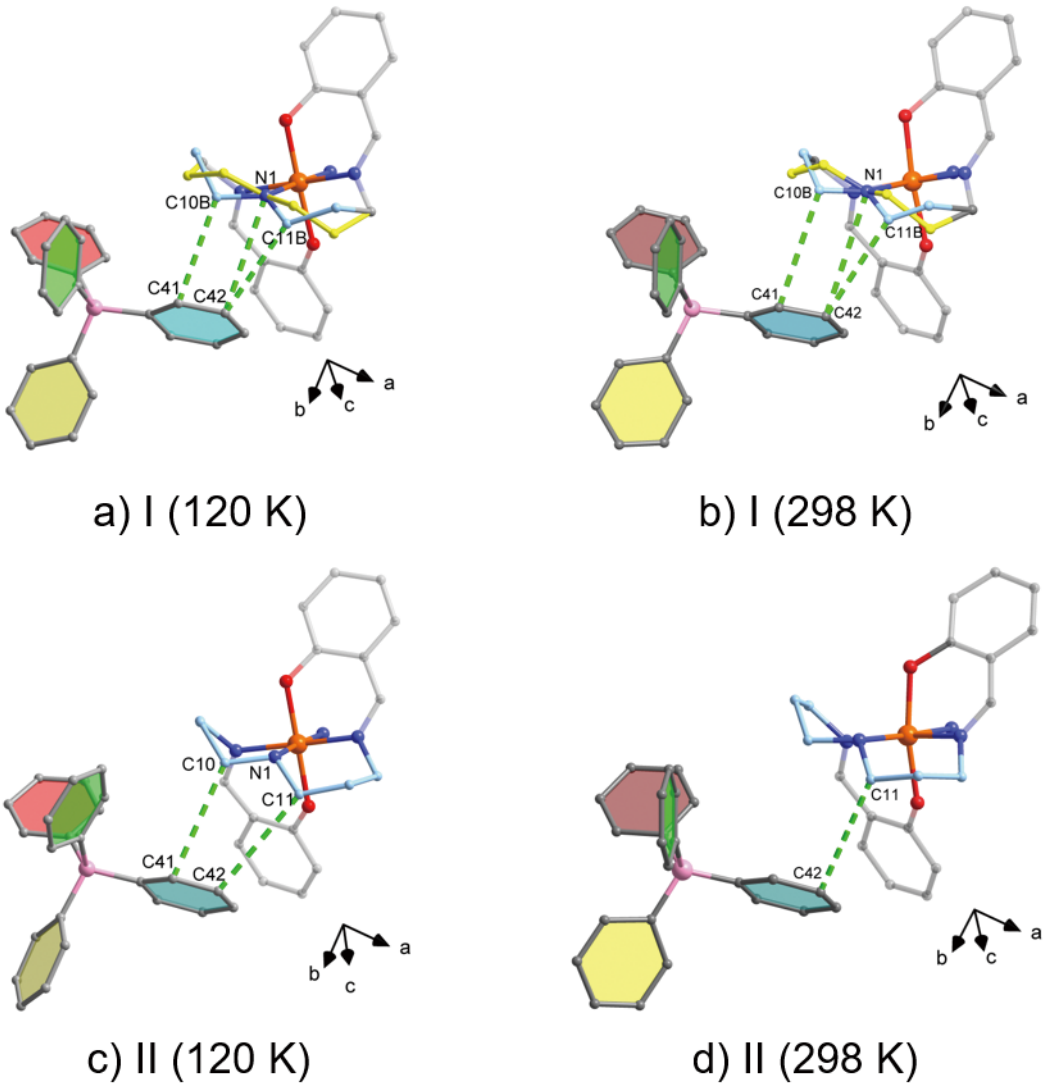


**Figure S7.** The intermolecular interactions between phenyl (C40−C45) of $BPh_4^-$ anion and the adjacent $[\{Fe^{III}(salten)\}_2(TPB)]^{2+}$ for a) **I** at 120 K, b) **I** at 298 K, c) **II** at 120 K and d) **II** at 298 K.

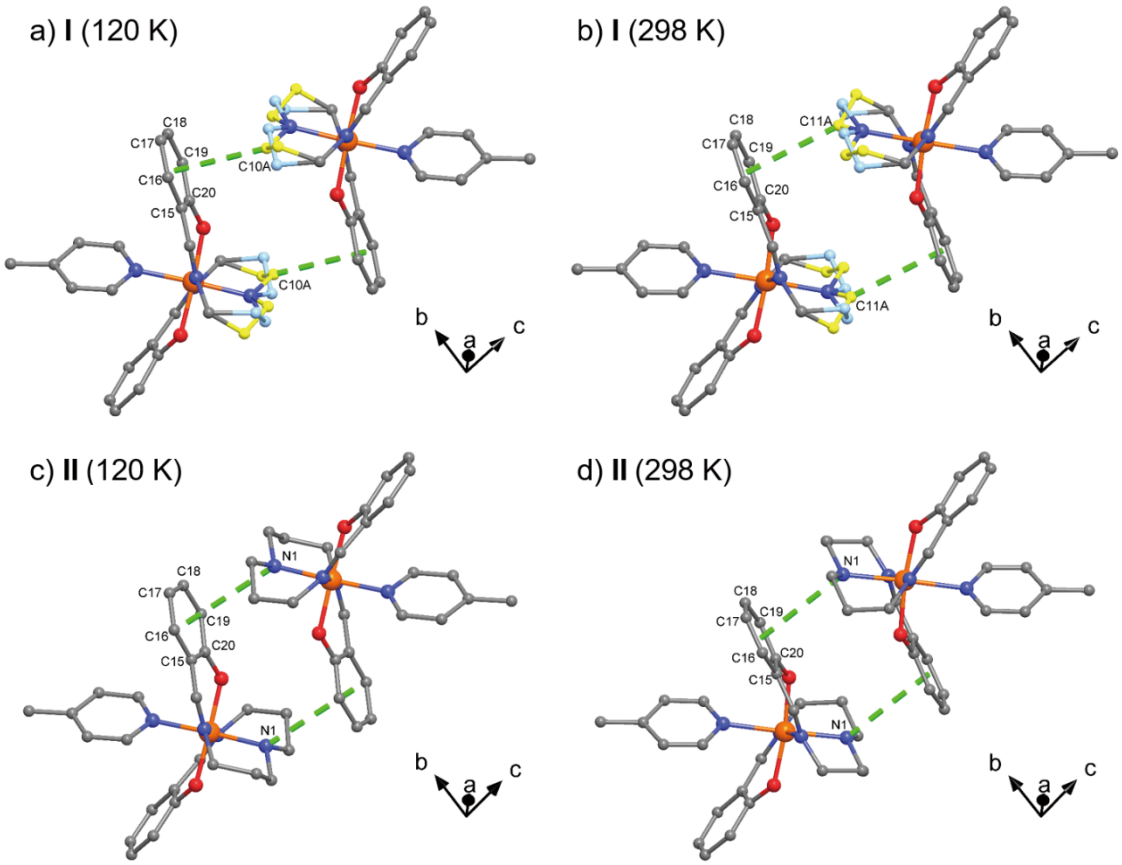


**Figure S8.** The intermolecular interactions between the adjacent $[\{Fe^{III}(salten)\}_2(TPB)]^{2+}$ for a) **I** at 120 K, b) **I** at 298 K, c) **II** at 120 K and d) **II** at 298 K. The dash lines represent for shortest distance among cations.

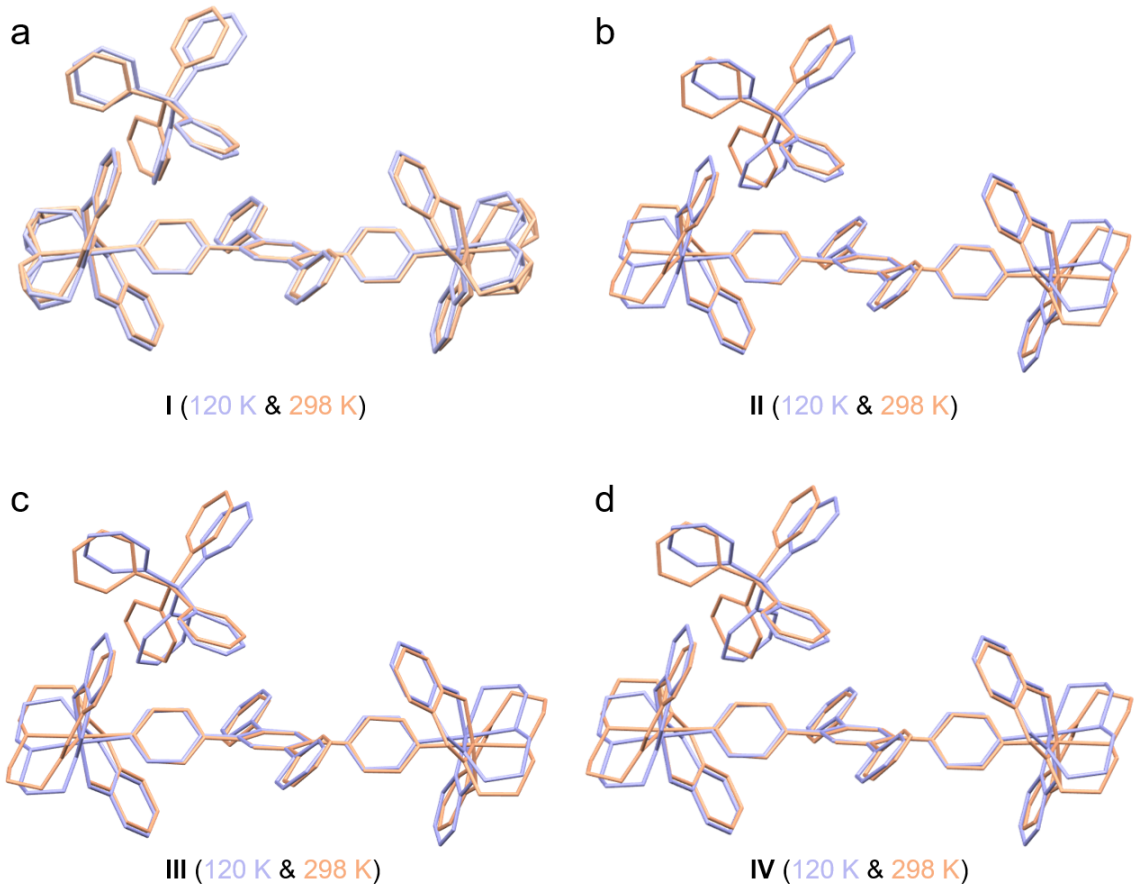


**Figure S9.** Crystal structure overlap of HS (298 K, orange) and LS (120 K, purple) states.

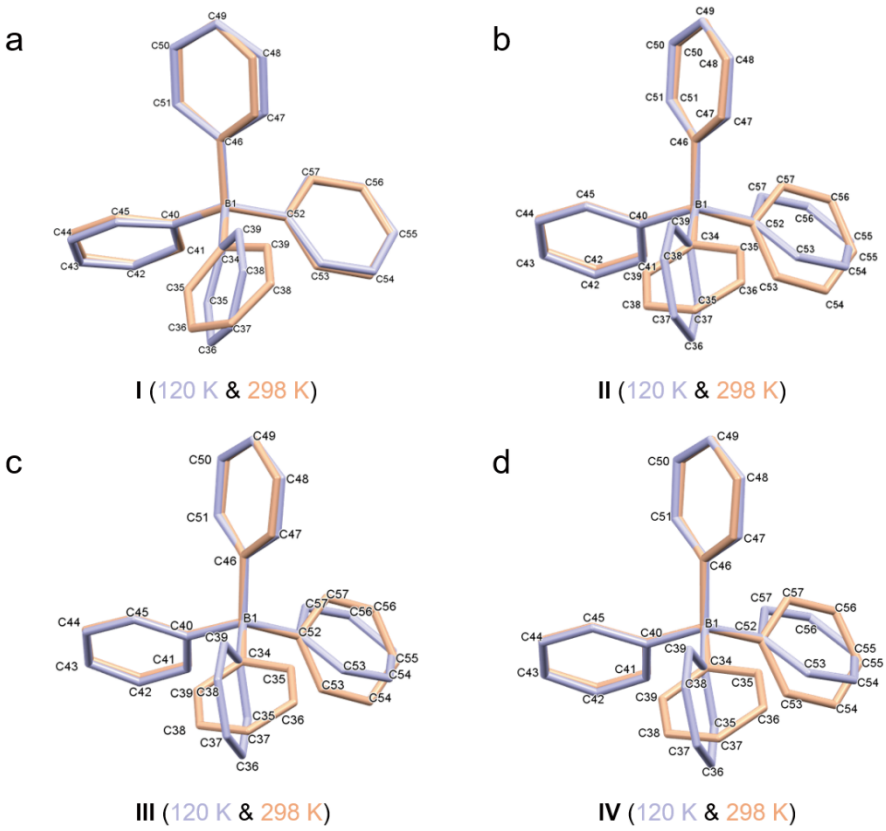


**Figure S10.** Structure overlap of $BPh_4^-$ anion at 120K (purple) and 298 K (orange): a) **I**, b) **II**, c) **III** and d) **IV**. B1, C34, C40, C46 and C52 are selected as reference points.

**Table S8.** Angles of two planes formed by same phenyl at two spin states.

| | C34−C39 | C40−C45 | C46−C51 | C52−C57 |
|---|---|---|---|---|
| **I** | 37.72 | 4.71 | 12.83 | 6.42 |
| **II** | 89.58 | 1.86 | 5.43 | 36.56 |
| **III** | 89.70 | 1.61 | 5.92 | 36.24 |
| **IV** | 89.78 | 1.58 | 5.34 | 36.39 |

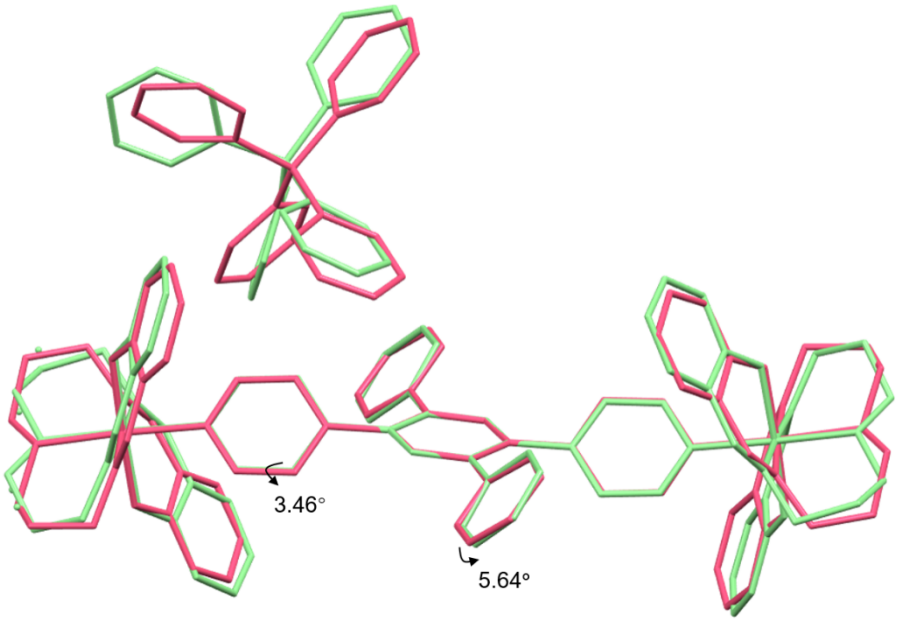


**Figure S11.** Crystal structure overlap of **I** (green) and **II** (red) at 120 K. The phenyl of TPB ligand is selected as reference points.

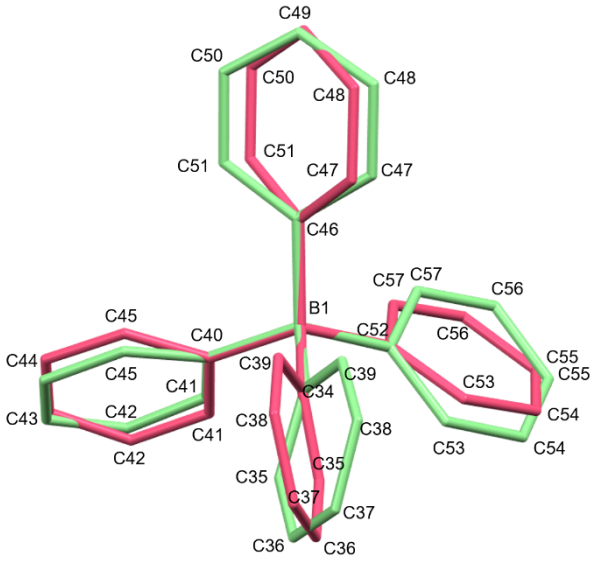


**Figure S12.** Structure overlap of $BPh_4^-$ anion in **I** (green) and **II** (red) at 120 K. B1, C34, C40, C46 and C52 are selected as reference points.

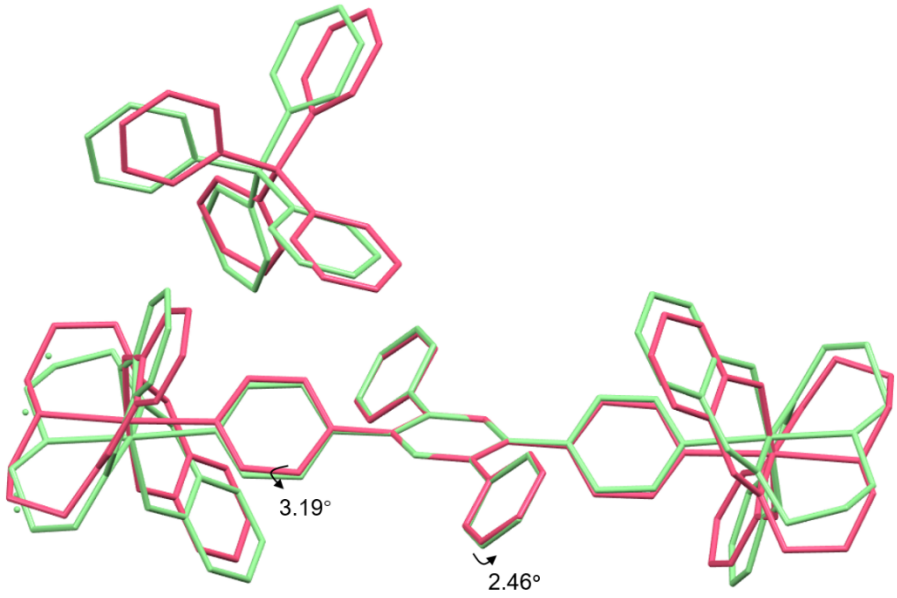


**Figure S13.** Crystal structure overlap of **I** (green) and **II** (red) at 298 K. The phenyl of TPB ligand is selected as reference points.

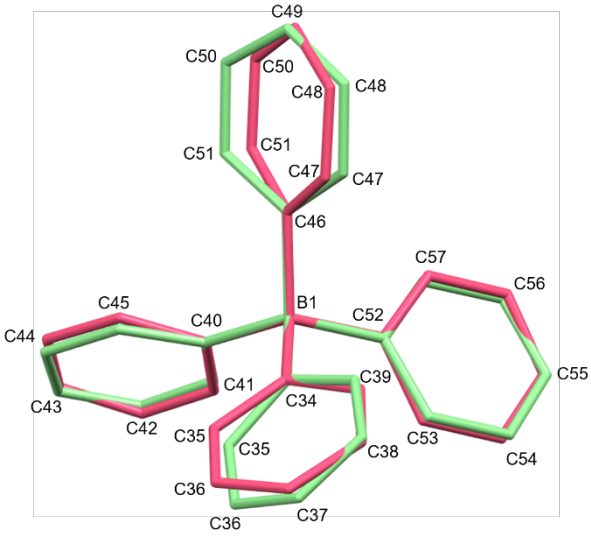


**Figure S14.** Structure overlap of $BPh_4^-$ anion in **I** (green) and **II** (red) at 298 K. B1, C34, C40, C46 and C52 are selected as reference points.

**Table S9** Angles of the two planes formed by same phenyl in different phases.

| Temperture [K] | | C34−C39 | C40−C45 | C46−C51 | C52−C57 |
|---|---|---|---|---|---|
| 120 | **I & II** | 41.03 | 13.87 | 30.38 | 21.23 |
| | **II & III** | 0.2 | 0.28 | 0.14 | 0.11 |
| | **II & IV** | 0.17 | 0.06 | 0.54 | 0.15 |
| 298 | **I & II** | 14.75 | 8.64 | 22.93 | 9.09 |
| | **II & III** | 0.23 | 0.21 | 0.26 | 0.30 |
| | **II & IV** | 0.07 | 0.46 | 0.07 | 0.28 |

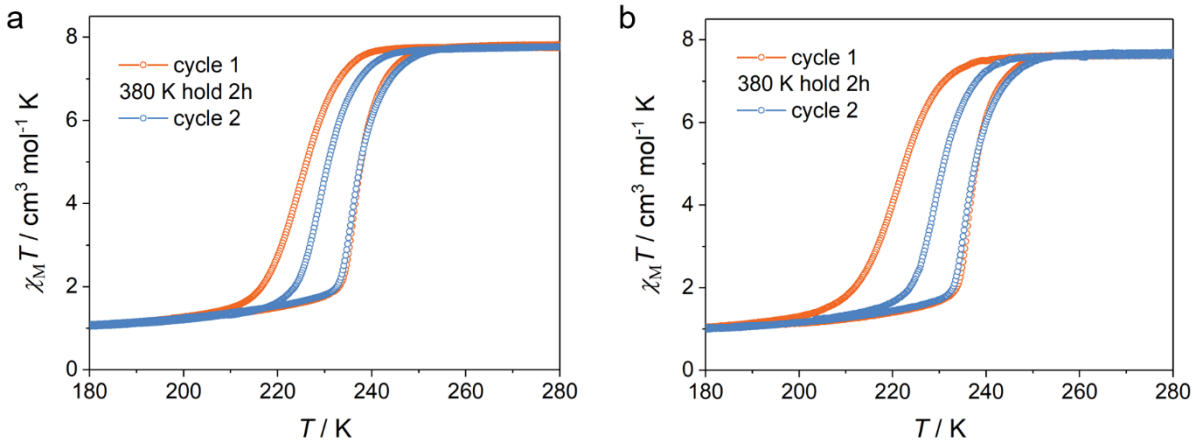


**Figure S15.** Variable-temperature magnetic susceptibilities transformation from a) **IV** to **II** and b) **III** to **II**.

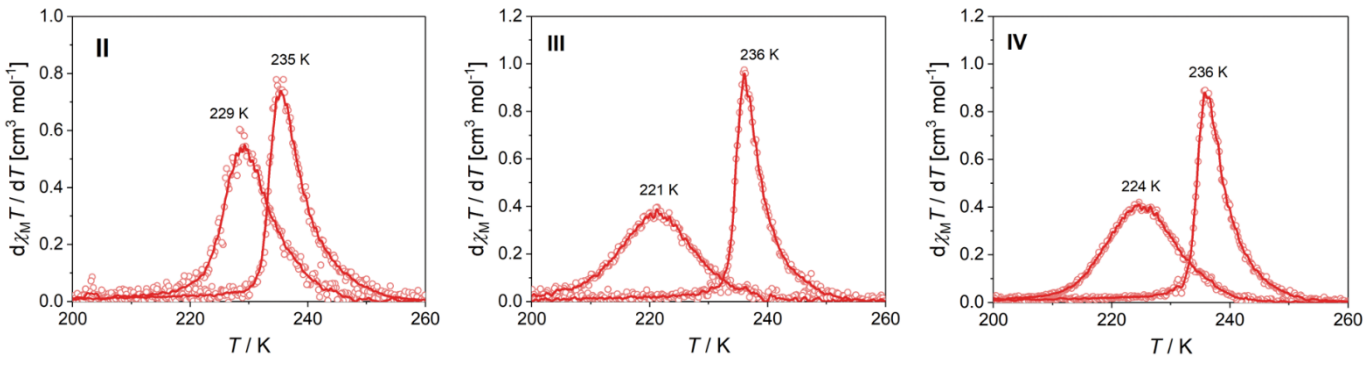


**Figure S16.** Differential of Variable-temperature magnetic susceptibilities for a) **II**, b) **III**, c) **IV**.

## Density Functional Theory Calculations

Investigation of the spin multiplicity of individual Fe sites in the $Fe_2$ compounds using a reduced structure

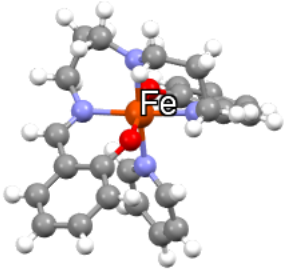


**Figure S17.** Example of the reduced structure of the compounds investigated. The closest pyridine ligand from the bridging ligand was kept, while the remaining site of the molecule was deleted. The dangling bond of the remaining pyridine ligand was saturated by a H atom.

As the molecules were found to have inversion symmetry, only half of the molecules is needed for calculation. The new reduced structures have only 1 metal centre (Figure S18). The DFT calculation was done using ORCA with the following parameters:

- DFT functional: B3LYP
- Basis set: DKH-def2-TZVP SARC/J
- Dispersion correction: D3BJ
- Convergence strategies: TightSCF
- Grid: Grid7 FinalGrid7
- Charge of compound: 1; multiplicity was varied between 2, 4, and 6 as the possible spin states for $Fe^{III}$ is 1/2, 3/2, 5/2.

**Table S10.** Energy calculated from a single-point-calculation of 8 reduced structures.

| Structure | Spin Multiplicity | Energy ($cm^{-1}$) |
|---|---|---|
| **I** at120K | 2 | 0.0 |
| | 4 | 6284.9 |
| | 6 | 9862.6 |
| **I** at 298K | 2 | 0.0 |
| | 4 | 1623.0 |
| | 6 | 404.9 |
| **II** at 120K | 2 | 0.0 |
| | 4 | 5547.8 |
| | 6 | 9259.9 |
| **II** at 298K | 2 | 2003.6 |
| | 4 | 2199.6 |
| | 6 | 0.0 |
| **III** at 120K | 2 | 0.0 |
| | 4 | 5636.6 |
| | 6 | 9475.8 |
| **III** at 298K | 2 | 2104.6 |
| | 4 | 2271.2 |
| | 6 | 0.0 |
| **IV** at 120K | 2 | 0.0 |
| | 4 | 6043.1 |
| | 6 | 9980.4 |
| **IV** at 298K | 2 | 1747.2 |
| | 4 | 2047.9 |
| | 6 | 0.0 |

## Investigation of the spin multiplicity of individual Fe site using the full molecular structure

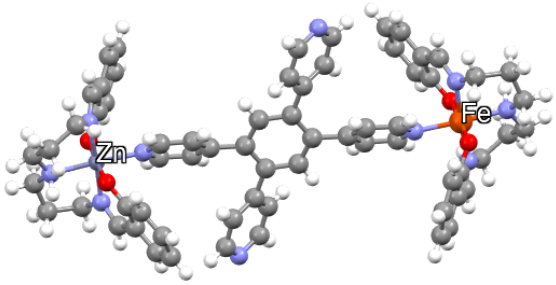


**Figure S18.** Example of the structure of the compounds investigated with one Fe replaced by Zn.

One Fe was replaced by Zn (Figure S18), while the remaining part of the molecule was kept intact, as in X-Ray structure. The calculation was done using ORCA-4.0.1 using the following parameters:

- DFT functional: B3LYP
- Basis set: DKH-def2-SVP SARC/J
- Dispersion correction: D3BJ
- Convergence strategies: TightSCF
- Grid: Grid7 FinalGrid7
- Charge of compound: +2; multiplicity was varied between 2, 4, and 6 as the possible spin states for $d^5$ configuration of $Fe^{III}$ is 1/2, 3/2, 5/2.The calculated energy of the single point calculation is shown in the table below. It was found that the multiplicities of both sites of Fe are the same within the same compound. Additionally, it is also evident that for compound **II**, **III**, and **IV**, at low temperature, Fe has low spin and at high temperature, Fe has high spin. For compound **I**, both Fe have low spin at low temperature and at high temperature.

**Table S11.** Energy calculated from a single-point-calculation for each Fe site in each structure. The other Fe site was replaced by Zn.

| Zn position | Structure | Multiplicity | Energy ($cm^{-1}$) | Zn position | Structure | Multiplicity | Energy ($cm^{-1}$) |
|---|---|---|---|---|---|---|---|
| 0 (Investigating the spin of Fe at position 97) | **I** at 120K | 2 | 0.0 | 97 (Investigating the spin of Fe at position 0) | **I** at 120K | 2 | 0.0 |
| | | 4 | 6451.8 | | | 4 | 6451.3 |
| | | 6 | 10139.0 | | | 6 | 10138.5 |
| | **I** at 298K | 2 | 0.0 | | **I** at 298K | 2 | 0.0 |
| | | 4 | 1789.0 | | | 4 | 1804.2 |
| | | 6 | 484.6 | | | 6 | 484.9 |
| | **II** at 120K | 2 | 0.0 | | **II** at 120K | 2 | 0.0 |
| | | 4 | 5951.6 | | | 4 | 5951.9 |
| | | 6 | 9757.6 | | | 6 | 9757.5 |
| | **II** at 298K | 2 | 2013.4 | | **II** at 298K | 2 | 2013.1 |
| | | 4 | 2215.2 | | | 4 | 2215.3 |
| | | 6 | 0.0 | | | 6 | 0.0 |
| | **III** at 120K | 2 | 0.0 | | **III** at 120K | 2 | 0.0 |
| | | 4 | 6053.2 | | | 4 | 6051.4 |
| | | 6 | 9990.9 | | | 6 | 9988.7 |
| | **III** at 298K | 2 | 2116.5 | | **III** at 298K | 2 | 2116.2 |
| | | 4 | 2277.9 | | | 4 | 2278.4 |
| | | 6 | 0.0 | | | 6 | 0.0 |
| | **IV** at 120K | 2 | 0.0 | | **IV** at 120K | 2 | 0.0 |
| | | 4 | 6187.7 | | | 4 | 5873.8 |
| | | 6 | 10227.3 | | | 6 | 9911.7 |
| | **IV** at 298K | 2 | 1751.0 | | **IV** at 298K | 2 | 1750.8 |
| | | 4 | 2090.4 | | | 4 | 2090.2 |
| | | 6 | 0.0 | | | 6 | 0.0 |

## Investigation of the spin multiplicity of the binuclear {$Fe_2$} compounds

As established previously, both Fe in compound **II**, **III**, and **IV** have low spin at low temperature and high spin at high temperature and both Fe in compound **I** have low spin at low and high temperature. Thus, the total spin of each compound is varied as shown in the table below. At high temperature, compound **II**, **III**, and **IV** have a total spin of 5 and at low temperature, they have a total spin of 1. On the other hand, at both 120 K and 298 K, compound **I** have a total spin of 1.

It is then concluded that the magnetic change could possibly be from the transition from the enthalpy-favored low spin to the entropy-favored high spin at each Fe site.

The computational details are similar to previous section. The spin was varied between 0 and 1 or 0, 1, 2, 3, 4, and 5, accordingly for each compound.

**Table S12.** Energy calculated from a single-point-calculation of 8 structures.

| **Structure** | **Multiplicity** | **Energy ($cm^{-1}$)** |
|---|---|---|
| **I** at120K | 1 | 0.2 |
| | 3 | 0.0 |
| **I** at 298K | 1 | 0.0 |
| | 3 | 258.6 |
| **II** at 120K | 1 | 24.9 |
| | 3 | 0.0 |
| **II** at 298K | 1 | 19994.2 |
| | 3 | 3972.1 |
| | 5 | 4198.2 |
| | 7 | 4432.6 |
| | 9 | 2212.4 |
| | 11 | 0.0 |
| **III** at 120K | 1 | 0.0 |
| | 3 | 552.2 |
| **III** at 298K | 1 | 20319.0 |
| | 3 | 4175.6 |
| | 5 | 4366.2 |
| | 7 | 4563.6 |
| | 9 | 2277.9 |
| | 11 | 0.0 |
| **IV** at 120K | 1 | 0.0 |
| | 3 | 496.9 |
| **IV** at 298K | 1 | 19624.8 |
| | 3 | 3450.9 |
| | 5 | 3783.5 |
| | 7 | 4123.8 |
| | 9 | 2058.0 |
| | 11 | 0.0 |

**Investigation of the exchange interaction of the {$Fe_2$} compounds at low temperature (120K) using broken symmetry DFT (BS-DFT) calculation**

The calculation was done for the {$Fe_2$} compound I, II, III, and IV at 120K. The calculation was done using ORCA-4.0.1 using the following parameters:

- DFT functional: B3LYP
- Basis set: DKH-def2-TZVP SARC/J
- Dispersion correction: D3BJ
- Convergence strategies: TightSCF (for compound **III**, VerySlowConv was employed since SCF could not converge using tight convergence criteria)
- Grid: Grid7 FinalGrid7
- Charge of compound: 2.

**Table S13.** Interaction of {$Fe_2$} compound at low temperature (120 K).

| Structure | $E_{High\text{-}Spin} - E_{BrokenSym}$ ($cm^{-1}$) | $J(1)$[4-6] ($cm^{-1}$) | $J(2)$[7] ($cm^{-1}$) | $J(3)$[8,9] ($cm^{-1}$) |
|---|---|---|---|---|
| **I** | -0.18 | 0.18 | 0.09 | 0.18 |
| **II** | -0.58 | 0.58 | 0.29 | 0.58 |
| **III** | 4.92 | -4.92 | -2.46 | -4.92 |
| **IV** | 1.19 | -0.60 | -0.60 | -1.19 |

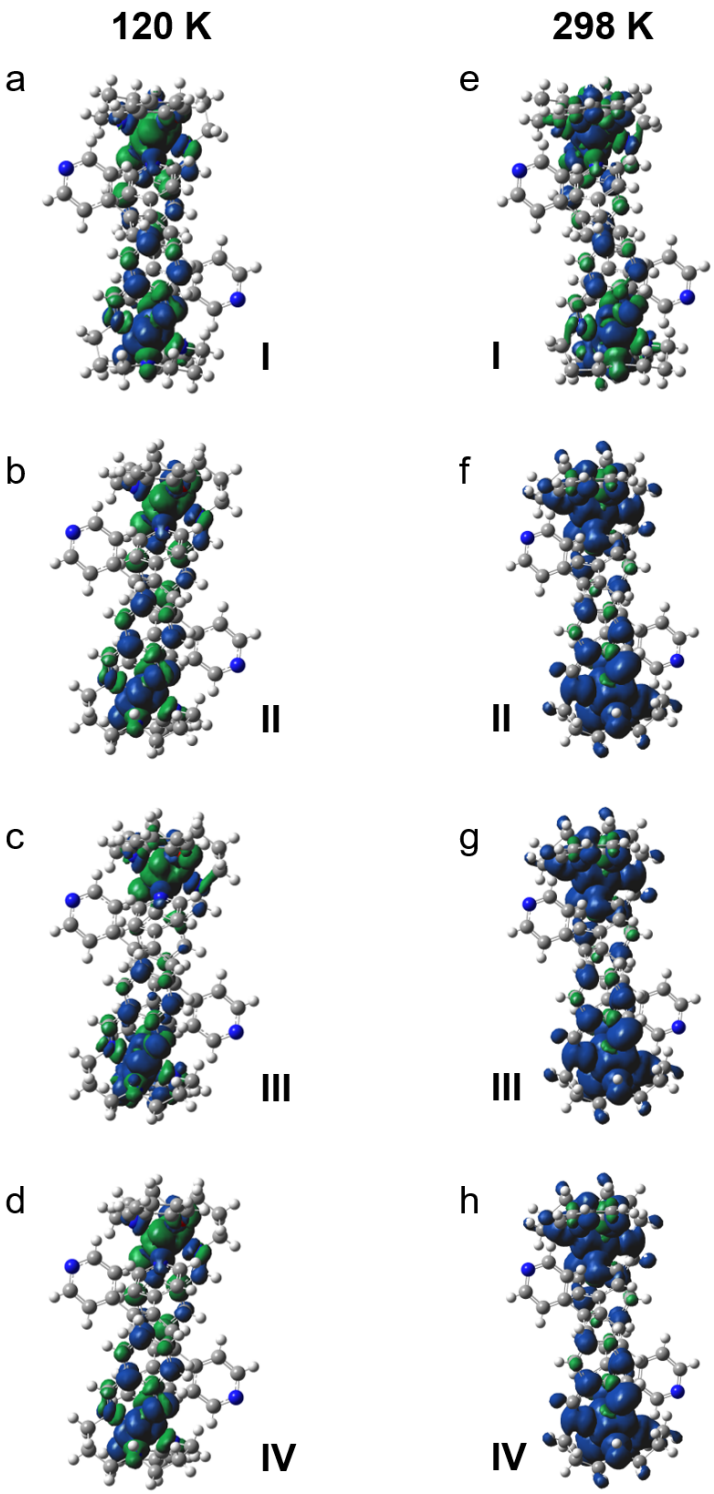


**Figure S19.** Spin density of the {$Fe_2$} compounds a) I at 120 K, b) II at 120 K, c) III at 120 K, d) IV at 120 K, e) I at 298 K, f) II at 298 K, g) III at 298 K, and h) IV at 298 K. The spin density of compound **I–IV** at 120 K was obtained from the result of the BS-DFT calculation. The spin density of compound **I–IV** at 298 K was obtained from the ground state result as shown in Table S12.

## References


1. Nemec, I.; Boča, R.; Gembický, M.; Dlháň, L.; Herchel, R.; Renz, F.; High-spin Schiff-base dinuclear iron(III) complexes bridged by N-oxide ligands. *Inorg. Chim. Acta* **2009**, *362*, 4754-4759.

2. Chang, Y.-C.; Wang, S.-L.; From Stimuli-Responsive Polymorphic Organic Dye Crystals to Photoluminescent Cationic Open-Framework Metal Phosphate *J. Am. Chem. Soc.* **2012**, *134*, 9848-9851.

3. Sheldrick, G.; A short history of SHELX. *Acta Cryst. A* **2008**, *64*, 112-122.

4. Ginsberg, A.; Magnetic exchange in transition metal complexes. 12. Calculation of cluster exchange coupling constants with the X.alpha.-scattered wave method. *J. Am. Chem. Soc.* **1980**, *102*, 111-117.

5. Noodleman, L.; Valence bond description of antiferromagnetic coupling in transition metal dimers. *J. Chem. Phys.* **1981,** *74*, 5737-5743.

6. Noodleman, L.; Davidson, E.R.; Ligand spin polarization and antiferromagnetic coupling in transition metal dimers. *Chem. Phys.* **1985,** *109,* 131-143.

7. Bencini, A.; Gatteschi, D.; X.alpha.-SW calculations of the electronic structure and magnetic properties of weakly coupled transition-metal clusters. The [Cu2Cl6]2- dimers. *J. Am. Chem. Soc.* **1980**, *108*, 5763-5771.

8. Yamaguchi, K.; Takahara, Y.; Fueno T.; Applied Quantum Chemistry. V.H. Smith (Ed.) *Reidel, Dordrecht* **1986**.

9. Soda, T.; Kitagawa, Y.; Onishi, T.; Takano, Y.; Shigeta, Y.; Nagao, H.; Yoshioka, Y.; Yamaguchi, K.; Ab initio computations of effective exchange integrals for H–H, H–He–H and Mn2O2 complex: comparison of broken-symmetry approaches. *Chem. Phys. Lett.* **2000,** *319*, 223-230.